JASA ARTICLE

Characterization of an underwater metamaterial made of aluminum honeycomb panels at low frequencies

Colby W. Cushing,[1,a)] Preston S. Wilson,[1,b)] Michael R. Haberman,[1,c)] Chen Shen,[2,d)] Junfei Li,[2,e)] Steven A. Cummer,[2] Zheng Jie Tan,[3] Chu Ma,[3,f)] Huifeng Du,[3] and Nicholas X. Fang[3]

[1]*Applied Research Laboratories and Walker Department of Mechanical Engineering, University of Texas, Austin, Texas 78713-8029, USA*

[2]*Department of Electrical and Computer Engineering, Duke University, Durham, North Carolina 27708, USA*

[3]*Department of Mechanical Engineering, Massachusetts Institute of Technology, Cambridge, Massachusetts 02139, USA*

ABSTRACT:

This paper presents a method to characterize the effective properties of inertial acoustic metamaterial unit cells for underwater operation. The method is manifested by a fast and reliable parameter retrieval procedure utilizing both numerical simulations and measurements. The effectiveness of the method was proved to be self-consistent by a metamaterial unit cell composed of aluminum honeycomb panels with soft rubber spacers. Simulated results agree well with the measured responses of this metamaterial in a water-filled resonator tube. A sub-unity density ratio and an anisotropic mass density are simultaneously achieved by the metamaterial unit cell, making it useful in implementations of transformation acoustics. The metamaterial, together with the approach for its characterization, are expected to be useful for underwater acoustic devices. © *2021 Acoustical Society of America*.

https://doi.org/10.1121/10.0003629

(Received 30 July 2020; revised 5 February 2021; accepted 15 February 2021; published online 16 March 2021)

[Editor: Olga Umnova] Pages: 1829–1837

I. INTRODUCTION

Recent years have witnessed a rapid development of acoustic metamaterials (AMMs), where their macroscopic properties are determined by the subwavelength inclusions within these structures (Cummer *et al.*, 2016; Ge *et al.*, 2018; Ma and Sheng, 2016). Numerous intriguing functionalities have been realized based on the exotic properties that AMMs can offer (Liu *et al.*, 2000; Shen *et al.*, 2015; Yves *et al.*, 2017; Zigoneanu *et al.*, 2014). Despite the abundant experimental proposals that work in air, successful demonstrations in water have been scarce (Bi *et al.*, 2017, 2018; Brunet *et al.*, 2015; Cai *et al.*, 2019; Fang *et al.*, 2006; Popa *et al.*, 2016; Zhang *et al.*, 2011). This is primarily due to the complexity of interactions between solids and dense fluids. For example, because of the relatively large characteristic impedance of water, few materials have sufficient impedance contrast to be considered acoustically rigid in water. This makes designs that work well in air, such as space-coiling structures (Liang and Li, 2012) or Helmholtz resonators (Kaina *et al.*, 2015), difficult to directly transfer to water, as the non-negligible impedance contrast of the solids must be included for accurate modeling.

Another difficulty encountered with underwater AMMs is the reduction of the effective shear modulus of the structures. It has been shown that a finite shear modulus will introduce undesired resonances that contaminate the effective properties of the metamaterials (Popa *et al.*, 2016; Smith and Verrier, 2011; Urzhumov *et al.*, 2010). For anisotropic metamaterials, non-negligible shear modulus will also significantly reduce the anisotropy ratio. Pentamode metamaterials composed of latticed filaments with solid inclusions that have vanishing shear modulus can be a potential solution (Chen *et al.*, 2017; Layman *et al.*, 2013; Norris, 2009; Su *et al.*, 2017). However, these metamaterials are composed of complicated structures and are not fabrication-friendly for large quantities. Consequently, these challenges severely hinder the applications of AMMs in water, such as medical ultrasound and underwater acoustic communications.

In addition to the difficulties in the design and fabrication of underwater AMMs, the field lacks methods that can numerically and experimentally characterize these metamaterials efficiently. To date, most metamaterials reported to operate in water involve relatively simple structures, such as layered metal sheets immersed in water (Bi *et al.*, 2017, 2018; Popa *et al.*, 2016). For more complicated structures, numerical simulations based on finite element analysis may be difficult due to the complexity induced by small features and solid-fluid interactions. On the other hand, an unbounded medium method has been proposed to experimentally estimate the effective properties of metamaterial blocks based on field mapping (Popa *et al.*, 2016). This

[a)]Electronic mail: colby.cushing@utexas.edu, ORCID: 0000-0002-3995-7390.
[b)]ORCID: 0000-0002-4420-7180.
[c)]ORCID: 0000-0002-7159-9773.
[d)]Current address: Department of Mechanical Engineering, Rowan University, 201 Mullica Hill Road, Glassboro, NJ 08028, USA, ORCID: 0000-0003-3535-8494.
[e)]ORCID: 0000-0002-5184-1737.
[f)]Current address: Department of Electrical and Computer Engineering, University of Wisconsin, Madison, WI 53706, USA.

method, however, requires the size of the metamaterial sample to be several wavelengths in order to perform field averaging. Consequently, a large water tank is required at low frequencies as the wavelength increases, and the field mapping can be time consuming.

In this paper, we describe a fast and reliable hybrid numerical/experimental method for the prediction of effective mass density and bulk modulus of underwater metamaterials. For the numerical part, a standard procedure was developed based on finite element analysis, which takes into account the solid-fluid interactions of the metamaterial structure while effectively minimizing the computational load. For the experimental part, we present a measurement procedure using a water-filled resonator adapted from previous work characterizing bubbly liquids (Dolder and Wilson, 2017), seagrass (Enenstein *et al.*, 2013; Johnson *et al.*, 2017), and water saturated glass beads (Venegas and Wilson, 2019). Other previous work had employed an impedance tube to characterize a layered metamaterial sample with a structure comprised of lossy sonic crystals for in-air applications (Guild *et al.*, 2015). However, water-filled impedance tubes are not readily available and cannot easily be constructed. Therefore, the methodology employed by Guild *et al.* was not used to characterize the effective properties of the underwater AMMs presented in this work. When the samples are loaded in the tube, the effective properties can be extracted by analyzing the mode frequency shift compared with the water-only resonator tube measurement. The use of aluminum honeycomb panels as building blocks of underwater metamaterials is also proposed. It is found that the honeycomb panels support a sub-unity density ratio in one direction as well as anisotropic mass densities in orthogonal directions.

The paper is organized as follows: The design and numerical simulations of the underwater metamaterial unit cell composed of aluminum honeycomb panels are presented in Sec. II. The measurement technique we used to characterize the metamaterial as well as the results obtained from the fabricated samples are shown in Sec. III. A summary and conclusions are presented in Sec. IV.

II. DESIGN AND NUMERICAL SIMULATIONS

The structure of the proposed metamaterial block is depicted in Fig. 1. It is composed of four aluminum honeycomb panels, which are interconnected by four soft rubber rods on the corners. Aluminum honeycomb panels are well known for their light weight and high mechanical stiffness (Ashby *et al.*, 2000; Zenkert, 1995). They have also been adopted in the acoustics community to construct light yet strong structures (Sui *et al.*, 2015; Wen-chao and Chung-fai, 1998). Compared with previous layered structures using dense materials, such as brass and steel (Bi *et al.*, 2017, 2018; Popa *et al.*, 2016), the use of aluminum honeycomb panels greatly reduces the overall weight without sacrificing stiffness. Another advantage is they can yield much smaller effective densities, which are crucial for application to transformation acoustics (Chen and Chan, 2010), as will be demonstrated later in this section. One important aspect of the design of the metamaterial is the control of the shear modulus, whose presence will degrade the performance of the metamaterial in water. For layered structures, it is ideal to have the individual layers suspended in water so that the shear stiffness of the overall structure is small. However, this will inevitably eliminate the ability of the structure to retain its shape. One approach to tackle this problem is to use rubber coated neodymium magnets (Popa *et al.*, 2016), but this adds fabrication complexity and still does not avoid the introduction of undesired resonances. Moreover, this solution is not compatible with non-magnetic materials such as the aluminum panels used in this work. We have therefore decided to use highly compliant rubber rods to connect neighboring aluminum honeycomb panels. The rubber rods are stretched and fitted into the holes on the aluminum panels to make the entire structure retain its shape while providing a seal to minimize the possibility of water penetrating the cells of the honeycomb.

The detailed structure of the aluminum honeycomb panel is shown in Fig. 1(b). The panel is composed of a core honeycomb lattice bounded by two face sheets on the top and bottom sides. The thicknesses of the core layer and the face sheets are 8 and 0.8 mm, respectively. The side length

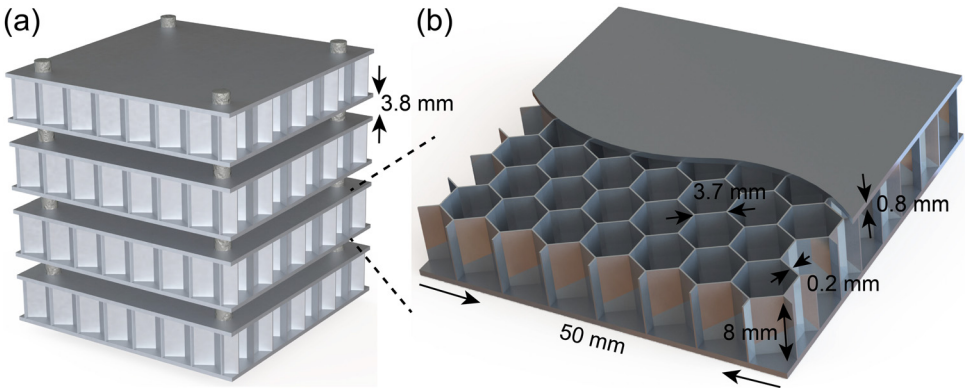

FIG. 1. (Color online) Illustration of the metamaterial. (a) The unit cell is composed of stacked aluminum honeycomb panels, which are connected by soft rubber rods to reduce the shear modulus. (b) Illustration of a honeycomb panel, which is a sandwiched structure consisting of a core honeycomb lattice and two face sheets.

https://doi.org/10.1121/10.0003629

of the hexagonal cell is 3.7 mm with thickness 0.2 mm. The thickness of a single assembled panel is 50 mm. The metamaterial unit cell is cubic with side length being 50 mm and is formed by evenly spacing four aluminum panels.

Numerical simulations based on finite element analysis were used to study the behavior of the metamaterial sample. For underwater operations, we are interested in the effective properties of the metamaterial unit cell, namely the effective mass density and sound speed in orthogonal directions. Although a typical parameter retrieval method has been established based on reflection and transmission coefficients (Fokin *et al.*, 2007), it is not trivial to directly apply this method to study the metamaterial under study, even numerically. This is because the honeycomb structure is complex with thin walls and small features, when compared to an acoustic wavelength, which require a high computational effort to be fully modeled. To tackle this issue, the procedure was broken down into two steps. A single honeycomb panel and its surrounding water layers is first simulated, including the exact inner structures, as shown in Fig. 2(a). The side length of the panel was reduced from 50 to 30 mm for improved computational efficiency. A set of simulations were then performed to determine the effective properties of the honeycomb panel itself, by comparing the simulated responses produced by the explicit structures to the response with effective properties. The thermoviscous effects were not included because the viscous boundary layer (Yazaki *et al.*, 2007) is much smaller than the separation between the plates. Therefore, their effects in such multilayered structures are neglected in the study. The variables referring to the effective material properties in the simulation are defined follows:

B = bulk modulus ratio of AMM compared to water,
$\rho_\perp$ = density ratio of AMM in perpendicular orientation compared to water,
$\rho_\parallel$ = density ratio of AMM in parallel orientation compared to water.

The best fit was sought such that the effective medium simulation and the explicit model produce the same response within the spectrum of interest. From Figs. 2(b) and 2(c), when the effective property ratios of the honeycomb panel are $\rho_\perp = 0.72$, $\rho_\parallel = 1.06$, and $B = 0.87$, agreement was observed. Note that throughout this paper, the effective material properties are all normalized to the density and bulk modulus of water, which are assumed to be 998 kg/m^3 and 2.23 GPa, respectively. This effective panel can later be integrated with water layers for the calculation of the effective properties of the assembled structures with various configurations. The effective properties inferred from the full structure simulations reveal some dispersion. However, because the dispersion was found to be less than 3%, the dispersion was ignored, and frequency independent effective properties at 3 kHz were used in simulation comparisons.

The inferred parameters are then used in a simulation of the full unit cell structure to calculate the overall effective properties of the metamaterial, as depicted in Fig. 3(a). Note that in this step, the panels are represented by effective media to facilitate the calculations. The inferred effective density and modulus of the metamaterial unit cell are shown in Figs. 3(b) and 3(c). It can be seen that the overall unit cell is anisotropic, with effective density ratios in the perpendicular and parallel direction being $\rho_\perp = 0.82$ and $\rho_\parallel = 1.04$, respectively. The anisotropy mainly stems from the structure of the assembled metamaterial, which results in different inertia of wave motion for the two orientations. Remarkably, the effective modulus ratio is $B = 0.92$, which indicates that the phase speed in the perpendicular direction is greater than water. The anisotropy ratio is dependent on the material properties of the constituent materials in such a multilayered structure and is limited in this work as the effective density of the honeycomb panels is close to water. To further increase the anisotropy ratio, lighter materials such as metal foams may be used (Popa and Cummer, 2011). Such sub-unity density and above-unity phase speed could be meaningful in designing transformation acoustics devices with better performance (Chen and Chan, 2010). For example, in the design of underwater cloaks (Bi *et al.*, 2017; Bi *et al.*, 2018; Kerrian *et al.*, 2019), the required effective densities are typically scaled up to facilitate the

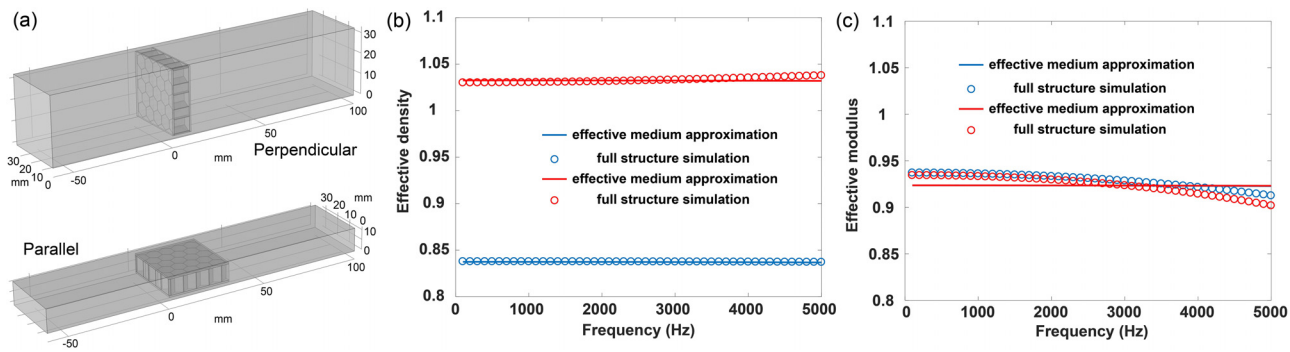

FIG. 2. (Color online) Determination of the effective property ratios of the honeycomb panels. (a) Finite element simulation in perpendicular and parallel orientations using an accurate representation of the internal honeycomb structure and the face sheets. The best fits between the full structure simulation and the effective medium approximations are shown. Outside the panel is water, and inside the honeycomb is air. (b) Best-fit effective density. (c) Best-fit effective bulk modulus. Blue: perpendicular direction. Red: parallel direction.

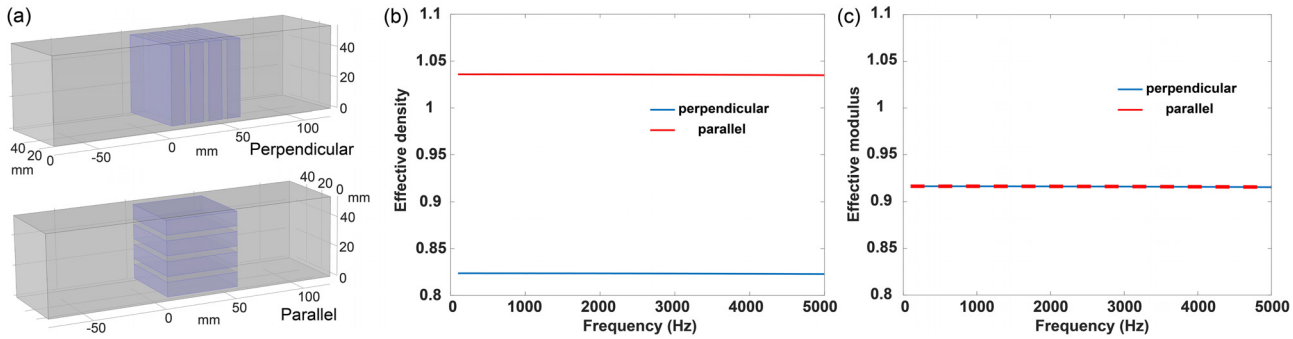

FIG. 3. (Color online) Determination of the effective properties of the metamaterial unit cell. (a) Finite element simulation in perpendicular and parallel orientations. The panels (represented by the blue-colored blocks) were modeled as anisotropic effective media in the simulations, and the gray-colored regions are water. (b) Inferred effective density in the two orientations. (c) Inferred effective bulk modulus in the two orientations.

design procedure, as it is difficult to realize sub-unity density materials. This, however, will inevitably introduce impedance mismatches and degrade the cloaking performance. Although strategies have been proposed using metal foams (Popa and Cummer, 2011) or elastic membranes (Shen *et al.*, 2014), they have yet to be experimentally verified. Our approach can therefore serve as an improved means to implement such devices.

Simulations were carried out to estimate the effective shear modulus of the metamaterial using elastic rubber rods. This was done by analyzing the shear strain γ when an in-plane shear stress τ was applied, as shown in Fig. 4. As the stiffness of the honeycomb panels is much larger than the rubber rods, the shear strain mostly comes from the displacement of the rubber rods. This in turn reduces the overall shear modulus of the metamaterial unit cell. The rubber rods had a 1.6 mm radius and a 3.87 mm length. The density, Young's modulus, and Poisson's ratio of the rubber were 1522 kg/m^3, 1.35 MPa, and 0.499, respectively. The effective shear modulus was then derived by $G = \tau/\gamma$, which yielded 48.8 kPa. According to previous literature (Chen *et al.*, 2015; Smith and Verrier, 2011; Urzhumov *et al.*, 2010), this effective shear modulus (<1% of the corresponding bulk modulus of the background fluid) is well within the range for the suppression of unwanted resonances. Therefore, it is expected that the use of rubber rods provides a reliable means for the connection between individual panels while maintaining low shear modulus. Note that the water layers between the honeycomb panels provide compressional stiffness close to that of water.

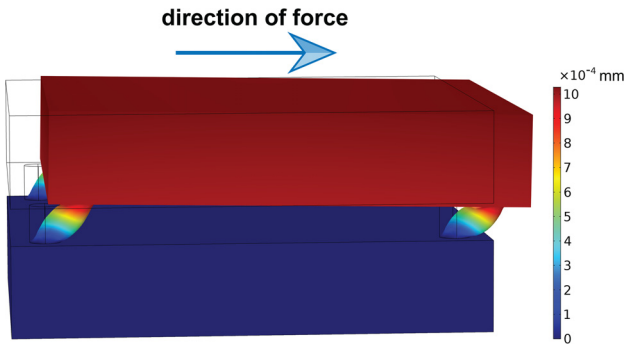

FIG. 4. (Color online) Analysis of the effective shear modulus between layers. The displacement field can be obtained numerically by applying shear force on one of the faces.

III. EXPERIMENTAL CHARACTERIZATION OF THE UNDERWATER METAMATERIAL

Three of the unit cells described in Sec. II were constructed and experimentally characterized using a one-dimensional (1-D) resonator tube approach. A 0.615-m-long glass-walled tube (wall thickness 4.7 mm) was used to determine dynamic effective sound speeds and densities of the materials. Figures 5 and 6 show the experimental setup with a representative tube and signal flow chart shown in Fig. 5. Three metamaterial unit cells are immersed inside the tube. To eliminate entrained air bubbles, the tube must be filled with degassed water with submerged samples left inside for several hours before testing. The degassing process allows for any trapped air in small crevices around the sample to diffuse back into solution, thus eliminating unwanted bubble effects. Since the unit cells are lighter than water, the

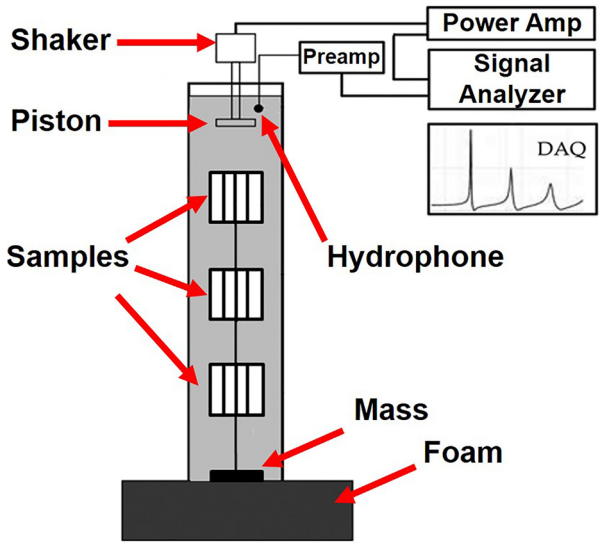

FIG. 5. (Color online) A representative resonance tube is shown with components labeled. Water-filled channels inside the unit cells are shown oriented in parallel to the acoustic axis of the waveguide.

https://doi.org/10.1121/10.0003629

samples were tethered using nylon monofilament to a ballast mass in the form of a large brass washer as shown in Fig. 5. The individual unit cells can also be tethered with the water layers oriented in the direction perpendicular to that shown in Fig. 5. These orientations correspond with the simulation orientation representations in Fig. 2.

An exponential chirp with frequency 0.05–10 kHz was used to excite the tube via an electromechanical shaker attached to a piston, as shown in Fig. 5. A RESON (Slangerup, Denmark) TC4013 hydrophone sensed the acoustic pressure response, which was recorded by a Data Physics (San Jose, CA) Quattro data acquisition system along with the excitation signal, and a transfer function was calculated using the Data Physics software. At each orientation, ten transfer functions were averaged in the frequency domain. These averaged transfer functions are referred to hereafter as the system response. The temperature of the water in the tube was measured using a thermocouple and recorded after every test-run and used to determine the sound speed of the water from Eq. (5.22) in Kinsler *et al.* (1999). The average temperature of the water over all experiments was approximately 22 °C. There were typical fluctuations of ±2 °C, depending on the time of day and the lab ventilation system reacting to outside weather conditions.

The air-water interface at the top of the tube is a close approximation of a pressure release boundary condition. The bottom surface was placed on a Styrofoam layer, which also approximates a pressure release boundary condition. A typical measured system response is shown in Fig. 7, where evenly spaced resonance peaks can be observed. Due to the pressure release conditions at both ends of the pipe, resonances occur at integer multiples of a half-wavelength ($\lambda/2 = L$). Rearranging this relationship, the sound speed can be calculated in terms of the length of the tube and frequency of the resonance. The frequencies of the resonance peaks and, subsequently, the sound speeds relating to the

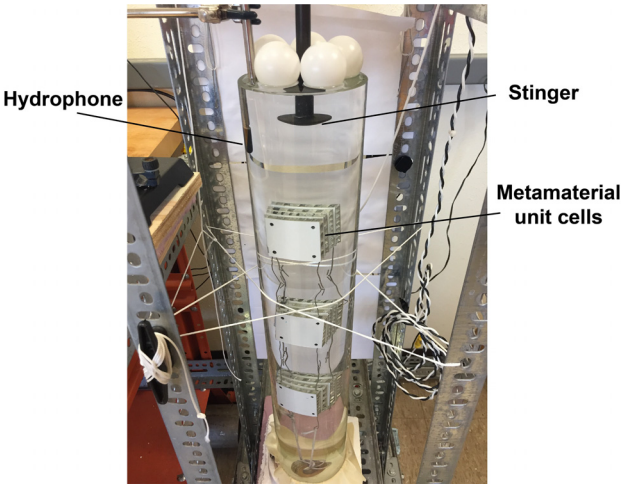

FIG. 6. (Color online) Experimental apparatus. A mechanical shaker was used to generate signals. The response was measured by a hydrophone. Three unit cells are shown suspended in the resonator.

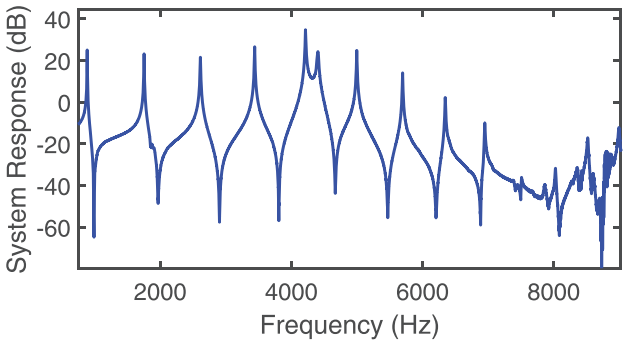

FIG. 7. (Color online) An example of a measured system response with the resonator filled with water and no unit cells. The first five resonance peaks are due to the first five plane wave-like modes. The sixth peak is a resonance due to shaker-stinger-piston structure. The next four higher modes are a continuation of the plane wave modal structure.

modes of vibration of the tube peaks are dependent upon the physical properties of the medium inside the tube. By changing the material in the tube in controlled volume fractions, the sound speed changes can be observed in the system response. If an appropriate mixture model is used to homogenize the water-material combination, the dispersion properties of the elastic tube wall can be accounted for, and the material properties of the foreign addition can be inferred. The materials used in the experiment are designed to be anisotropic, and therefore, the samples are tested in different orientations. Three separate tests were performed to characterize the metamaterial, including a water-filled case (no metamaterial samples) and tests for the parallel and perpendicular metamaterial orientations. Orientations are labeled with respect to direction of the particle velocity through the sample in the resonator tube, as shown in Fig. 3, and correspond to the directions shown in Fig. 2. For future experiments, it may be possible to orient the samples at a known angle with respect to the direction of the standing waves in the resonance tube in the simulation and resonator tube experiment. It is theoretically possible to orient the samples at a known three-dimensional angle such that the off-axis effective dynamic inertia could be compared between experiment and simulation to check the consistency of the system.

A. Inference of acoustic properties

A theoretical framework is outlined here to infer the acoustic properties of the metamaterial from measured data. The first step is to apply an appropriate mixing model for the water-metamaterial mixture as a function of volume fraction, density, and sound speed of both the metamaterial samples and water. The second step is to correct for the dispersion effects of the elastic-walled waveguide using an exact analytic expression developed by Del Grosso (1971) as well as Lafleur and Shields [Eq. (5) of Lafleur and Shields (1995)]. The mixture law developed by Mallock and Wood (Mallock, 1910; Wood, 1930) was used to represent the combination of materials in the tube as seen in Eq. (1):

$$\rho_{\text{mix}} = \rho_l(1-\chi) + \chi\rho_{\text{AMM}}$$
$$\frac{1}{K_{\text{mix}}} = \frac{(1-\chi)}{K_l} + \frac{\chi}{K_{\text{AMM}}} \quad (1)$$
$$c_{\text{mix}} = \sqrt{\frac{K_{\text{mix}}}{\rho_{\text{mix}}}},$$

where

ρ_l = density of water,
χ = volume fraction of the AMMs,
ρ_{AMM} = effective dynamic density of the AMM,
K_l = bulk modulus of water,
K_{AMM} = bulk modulus of AMM, assigned to be simulated value found in Sec. II,
ρ_{mix} = density of the water-AMM mixture,
K_{mix} = bulk modulus of the water-AMM mixture,
c_{mix} = longitudinal sound speed of the water-AMM mixture.

The volume fractions are known by measuring the volume of each sample and dividing by the internal volume of the tube. The bulk modulus of the AMM from the simulation in Sec. II is assumed to be constant for the experiment and was used as an input to the mixture model.

The effective properties from the mixture model were used as inputs to the dispersion expression found in Eq. (5) in Lafleur and Shields (1995), which is expressed in compact form by

$$c_{0,0} = f(c_{\text{mix}}, \rho_{\text{mix}}, \omega, b, d, Y, \rho_{\text{t}}, \nu), \quad (2)$$

where $c_{0,0}$ is the planar longitudinal phase speed in the waveguide, c_{mix} and ρ_{mix} are as defined by the Mallock–Wood mixture model in Eq. (1), ω is frequency, b is the inner radius of the tube, and d is the outer radius of the tube. Referring to the tube wall material, Y is the Young's modulus, ρ_{t} is the density, and ν is Poisson's ratio. The dynamic effective density of the metamaterial is the inferred property of the system, which is varied as an input to Eq. (1) until the left-hand side of Eq. (2) agrees with the sound speeds measured in the experiment. The free space effective sound speed of the metamaterial is then calculated using $c_{\text{AMM}} = \sqrt{K_{\text{AMM}}/\rho_{\text{AMM}}}$ and normalized by the sound speed of the water during the time that experiment was run. The latter was determined by measuring the temperature and using Eq. (5.22) of Kinsler *et al.* (1999). In its current form, the resonator tube method does not allow for simultaneous determination of the bulk modulus and effective dynamic density. In previous work that utilized the same experimental method, local inertia of the material of interest was very well approximated as being independent of frequency and orientation in the standing wave field of the resonator tube (Dolder and Wilson, 2017; Enenstein *et al.*, 2013; Johnson *et al.*, 2017). By extension, the dynamic density was well approximated by static tests, which permit the inference of bulk modulus or related material properties.

The effective local inertia of the AMM in the current work is direction-dependent and therefore dependent on orientation in the resonator tube. The inherent nature of the anisotropic effective dynamic density therefore defines the effective bulk modulus as being the inferred material property. Experimental measurement of the effective bulk modulus of the honeycomb panel assembly would be required to be made underwater as the heterogeneous inclusion relies on alternating water layers necessary for expected performance. The experimental apparatus as presented in this work is not yet equipped to independently determine the effective bulk modulus but could be considered in future work. Depending on the process employed, the tabulated effective sound speeds and effective dynamic densities would have to be adjusted to include inevitable error that would be present in experimentally verifying the bulk modulus of the AMM. In lieu of using an experimental process, the effective bulk modulus was approximated with a harmonic volumetric mean rule-of-mixtures relationship from a COMSOL representation of the AMM found in Sec. II.

B. Results

Figure 8(a) shows the system responses for the three separate cases, and Figs. 8(b) and 8(c) illustrate the peak frequency shifts in modes 1 and 3. The system responses for both orientations remain plane wave-like, similar to the water-only case, with no spurious resonances due to the AMM structure. It can be observed that the peak frequency shifts rightward and leftward at perpendicular and parallel orientations, respectively, which indicates above-unity and sub-unity sound speed ratios in these orientations. Figure 9

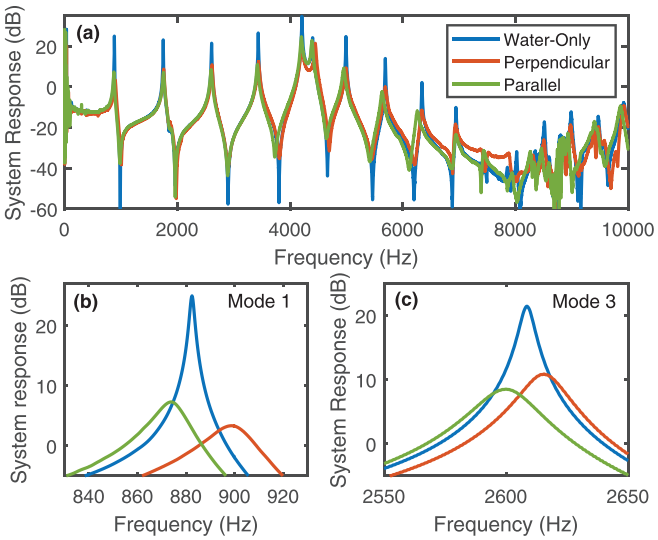

FIG. 8. (Color online) Measurement transfer function amplitudes are plotted for three cases: water only (blue), perpendicular orientation (red), and parallel orientation (green). (a) The full system response over the entire frequency range of the exponential chirp energizing the system via the stinger. The detailed views of the resonance peaks of the first and third modes are shown in (b) and (c), respectively.

https://doi.org/10.1121/10.0003629

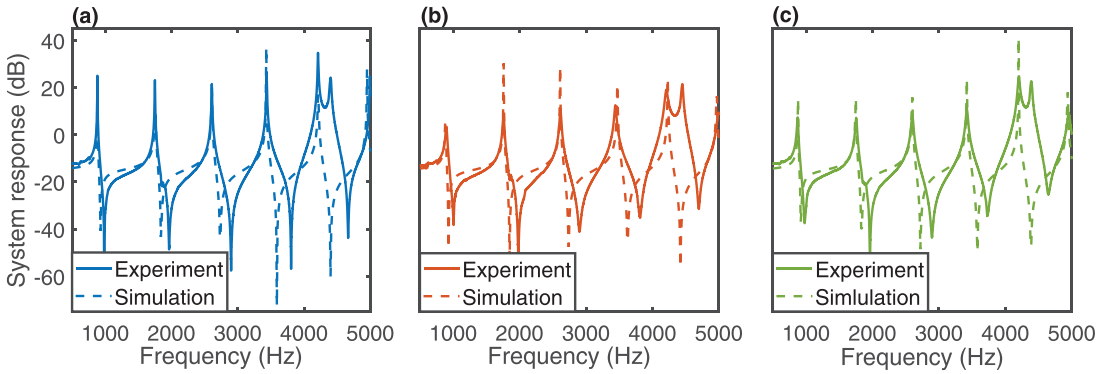

FIG. 9. (Color online) Comparison between simulated and measured system responses. (a) Water-only case. (b) Perpendicular orientation. (c) Parallel orientation.

compares the experimental transfer functions to the simulated systems. Higher-order non-plane modes exist in this system above 5000 Hz. For this reason, only the first five modes were used in the analysis. Good agreement can be found where the mode peaks are well captured by the simulation results, although disagreements exist in the nulls of the system responses. A resonance peak associated with a natural vibrational mode of the stinger is present immediately after mode 5 in all experimental data sets shown in Fig. 9. The stinger mode is absent from the corresponding simulations because the stinger was not included in the simulated system. The resonance extraction and subsequent material property inference detailed in Sec. III A show self-consistency in our numerical and experimental approach to the determination of the effective properties of the metamaterial. The measured resonance frequencies and the resulting sound speed ratios are shown in Table I.

By changing the AMM material property values as inputs to the Mallock–Wood mixture model representing the water-AMM mixture, new values are produced for c_{mix} and ρ_{mix}, which are inputs to Eq. (1). Equation (1) results, which are represented by the model curves in Fig. 9, are adjusted indirectly through the AMM material properties until the Eq. (1) curves align with experimental data points. The effective densities were found to be 863 and 1030 kg/m^3 for the perpendicular and parallel cases, respectively. The effective sound speeds of the metamaterial were found to be 1523 m/s for the perpendicular orientation and 1394 m/s for the parallel orientation. The bulk modulus of the material was assumed to be the simulated value found in Sec. II: $K_{\mathrm{AMM}} = 0.87K_l$. The value was assumed constant regardless of orientation because the simulations found negligible changes in bulk modulus as a function of frequency between the parallel and perpendicular cases. Further, this is in agreement with the assumption that the AMM structure produces an effective fluid with anisotropic effective dynamic density. A comparison between the experimental value and the simulated values can be found in Table II. Overall, there is very good agreement between the simulated material properties and the inferred properties from the resonator tube experiment. Finally, the normalized measured phase speeds were plotted as a function of frequency along with the dispersion expression in Eq. (2) (Lafleur and Shields, 1995; Del Grosso, 1971) in Fig. 10.

TABLE I. Frequencies of the resonance peaks of the measured system responses and normalized phase speeds.

	Resonance frequencies (Hz)				
	Mode 1	Mode 2	Mode 3	Mode 4	Mode 5
Water	882.226	1749.414	2607.813	3434.961	4200.011
Perpendicular	899.805	1758.984	2615.820	3441.602	4208.203
Parallel	874.023	1754.688	2600.195	3421.094	4201.953
	Wave guide phase speed/Water sound speed				
Water	0.7271	0.7209	0.7164	0.7077	0.6923
Perpendicular	0.7420	0.7252	0.7190	0.7095	0.6940
Parallel	0.7215	0.7243	0.7155	0.7061	0.6938

IV. CONCLUSION

We have designed and experimentally demonstrated an underwater AMM composed of aluminum honeycomb panels and soft spacers immersed in water. Numerical and experimental approaches were developed to characterize the underwater metamaterial in the frequency range from 1 to 4 kHz. The results from the simulations and experiments demonstrate self-consistency between the inferred and predicted effective material properties. Notably, these approaches can be used at low frequencies, which is very convenient for other techniques, such as field mapping or standard reflection-transmission techniques.

The effective sound speed and density ratios compare the AMM effective material properties with those of the

TABLE II. Inferred and simulated values for sound speed and density of the metamaterial for both perpendicular and parallel cases. Inferred values use assumed constant bulk modulus determined in simulations.

	Perpendicular		Parallel	
	Sound speed (m/s)	Density (kg/m^3)	Sound speed (m/s)	Density (kg/m^3)
Simulated	1573	822	1402	1034
Inferred	1523	863	1394	1030

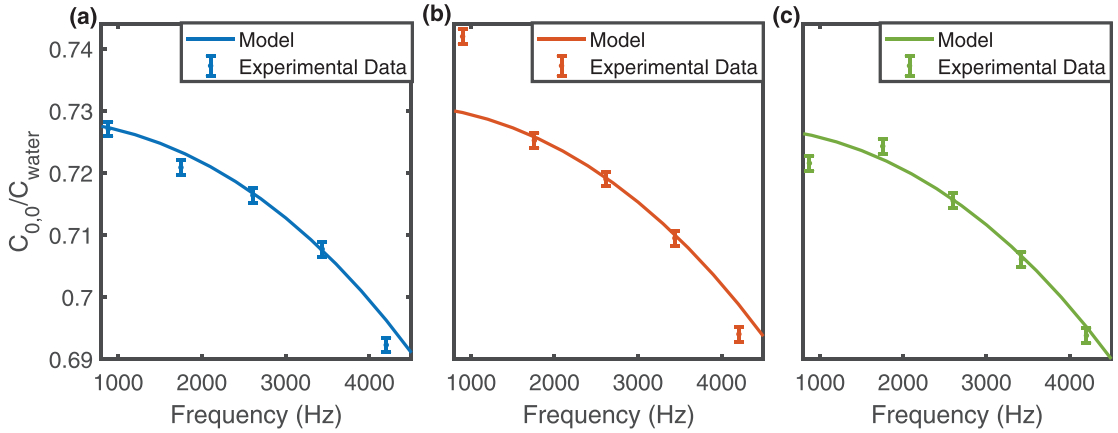

FIG. 10. (Color online) Demonstration of the self-consistency in the inference process: Measured and modeled waveguide dispersion for the water-filled tube (a) and the perpendicular (b) and parallel (c) metamaterial sample orientations. Error bars show measurement uncertainty due to uncertainties in the length of the waveguide and the finite frequency resolution of the measured transfer functions.

host medium. The AMM material properties of the unit cell building block are found to be above unity using water as a reference in the perpendicular direction, which is meaningful for the design of underwater devices based on transformation acoustics. The use of rubber rods as soft spacers not only provides an efficient means to connect the building blocks but also effectively reduces the shear modulus of the metamaterial and minimizes the interactions between adjacent layers. The aluminum honeycomb panels, which are employed as the main building blocks of the metamaterial, are low-cost and mechanically robust. It is hoped that the design strategy and characterization method presented in the paper can be helpful for designing future underwater metamaterials and novel acoustic devices.

ACKNOWLEDGMENTS

This work was supported by a Multidisciplinary University Research Initiative grant from the Office of Naval Research (Grant No. N00014-13-1-0631). C.W.C was supported by the McKinney Fellowship in Acoustics.

Ashby, M. F., Evans, T., Fleck, N. A., Hutchinson, J., Wadley, H., and Gibson, L. (**2000**). *Metal Foams: A Design Guide* (Elsevier, New York).
Bi, Y., Jia, H., Lu, W., Ji, P., and Yang, J. (**2017**). "Design and demonstration of an underwater acoustic carpet cloak," Sci. Rep. **7**(1), 705.
Bi, Y., Jia, H., Sun, Z., Yang, Y., Zhao, H., and Yang, J. (**2018**). "Experimental demonstration of three-dimensional broadband underwater acoustic carpet cloak," Appl. Phys. Lett. **112**(22), 223502.
Brunet, T., Merlin, A., Mascaro, B., Zimny, K., Leng, J., Poncelet, O., Aristégui, C., and Mondain-Monval, O. (**2015**). "Soft 3D acoustic metamaterial with negative index," Nat. Mater. **14**(4), 384–388.
Cai, Z., Zhao, S., Huang, Z., Li, Z., Su, M., Zhang, Z., Zhao, Z., Hu, X., Wang, Y.-S., and Song, Y. (**2019**). "Bubble architectures for locally resonant acoustic metamaterials," Adv. Funct. Mater. **29**(51), 1906984.
Chen, H., and Chan, C. T. (**2010**). "Acoustic cloaking and transformation acoustics," J. Phys. D Appl. Phys. **43**(11), 113001.
Chen, Y., Liu, X., and Hu, G. (**2015**). "Latticed pentamode acoustic cloak," Sci. Rep. **5**, 15745.
Chen, Y., Zheng, M., Liu, X., Bi, Y., Sun, Z., Xiang, P., Yang, J., and Hu, G. (**2017**). "Broadband solid cloak for underwater acoustics," Phys. Rev. B **95**(18), 180104.
Cummer, S. A., Christensen, J., and Alù, A. (**2016**). "Controlling sound with acoustic metamaterials," Nat. Rev. Mater. **1**(3), 16001.
Del Grosso, V. (**1971**). "Analysis of multimode acoustic propagation in liquid cylinders with realistic boundary conditions–application to sound speed and absorption measurements," Acta Acust. United Acust. **24**(6), 299–311.
Dolder, C. N., and Wilson, P. S. (**2017**). "Using one-dimensional waveguide resonators to measure phase velocities in bubbly liquids," J. Acoust. Soc. Am. **141**(4), 2832–2839.
Enenstein, G., Dolder, C., Wilson, P. S., and Hermand, J.-P. (**2013**). "Investigation of low-frequency acoustic tissue properties of seagrass," in *Proceedings of Meetings on Acoustics ICA2013*, Acoustical Society of America, Vol. 19, pp. 5–7.
Fang, N., Xi, D., Xu, J., Ambati, M., Srituravanich, W., Sun, C., and Zhang, X. (**2006**). "Ultrasonic metamaterials with negative modulus," Nat. Mater. **5**(6), 452–456.
Fokin, V., Ambati, M., Sun, C., and Zhang, X. (**2007**). "Method for retrieving effective properties of locally resonant acoustic metamaterials," Phys. Rev. B **76**(14), 144302.
Ge, H., Yang, M., Ma, C., Lu, M.-H., Chen, Y.-F., Fang, N., and Sheng, P. (**2018**). "Breaking the barriers: Advances in acoustic functional materials," Nat. Sci. Rev. **5**(2), 159–182.
Guild, M. D., García-Chocano, V. M., Kan, W., and Sánchez-Dehesa, J. (**2015**). "Acoustic metamaterial absorbers based on multilayered sonic crystals," J. Appl. Phys. **117**(11), 114902.
Johnson, J. R., Venegas, G. R., Wilson, P. S., and Hermand, J.-P. (**2017**). "Measurement of low-frequency tissue response of the seagrass posidonia oceanica," J. Acoust. Soc. Am. **141**(5), EL433–EL438.
Kaina, N., Lemoult, F., Fink, M., and Lerosey, G. (**2015**). "Negative refractive index and acoustic superlens from multiple scattering in single negative metamaterials," Nature **525**(7567), 77–81.
Kerrian, P. A., Hanford, A. D., Capone, D. E., and Beck, B. S. (**2019**). "Development of a perforated plate underwater acoustic ground cloak," J. Acoust. Soc. Am. **146**(4), 2303–2308.
Kinsler, L. E., Frey, A. R., Coppens, A. B., and Sanders, J. V. (**1999**). *Fundamentals of Acoustics* (John Wiley & Sons, Inc., Hoboken, NJ).
Lafleur, L. D., and Shields, F. D. (**1995**). "Low-frequency propagation modes in a liquid-filled elastic tube waveguide," J. Acoust. Soc. Am. **97**, 1435–1445.
Layman, C. N., Naify, C. J., Martin, T. P., Calvo, D. C., and Orris, G. J. (**2013**). "Highly anisotropic elements for acoustic pentamode applications," Phys. Rev. Lett. **111**(2), 024302.
Liang, Z., and Li, J. (**2012**). "Extreme acoustic metamaterial by coiling up space," Phys. Rev. Lett. **108**(11), 114301.
Liu, Z., Zhang, X., Mao, Y., Zhu, Y. Y., Yang, Z., Chan, C. T., and Sheng, P. (**2000**). "Locally resonant sonic materials," Science **289**(5485), 1734–1736.
Ma, G., and Sheng, P. (**2016**). "Acoustic metamaterials: From local resonances to broad horizons," Sci. Adv. **2**(2), e1501595.
Mallock, H. R. A. (**1910**). "The damping of sound by frothy liquids," Proc. R. Soc. Lond. A Math. Phys. Sci. **84**(572), 391–395.

Norris, A. N. (**2009**). "Acoustic metafluids," J. Acoust. Soc. Am. **125**(2), 839–849.
Popa, B.-I., and Cummer, S. A. (**2011**). "Homogeneous and compact acoustic ground cloaks," Phys. Rev. B **83**(22), 224304.
Popa, B.-I., Wang, W., Konneker, A., Cummer, S. A., Rohde, C. A., Martin, T. P., Orris, G. J., and Guild, M. D. (**2016**). "Anisotropic acoustic metafluid for underwater operation," J. Acoust. Soc. Am. **139**(6), 3325–3331.
Shen, C., Xie, Y., Sui, N., Wang, W., Cummer, S. A., and Jing, Y. (**2015**). "Broadband acoustic hyperbolic metamaterial," Phys. Rev. Lett. **115**(25), 254301.
Shen, C., Xu, J., Fang, N. X., and Jing, Y. (**2014**). "Anisotropic complementary acoustic metamaterial for canceling out aberrating layers," Phys. Rev. X **4**(4), 041033.
Smith, J. D., and Verrier, P. E. (**2011**). "The effect of shear on acoustic cloaking," Proc. R. Soc. Lond. A Math. Phys. Sci. **467**(2132), 2291–2309.
Su, X., Norris, A. N., Cushing, C. W., Haberman, M. R., and Wilson, P. S. (**2017**). "Broadband focusing of underwater sound using a transparent pentamode lens," J. Acoust. Soc. Am. **141**(6), 4408–4417.
Sui, N., Yan, X., Huang, T.-Y., Xu, J., Yuan, F.-G., and Jing, Y. (**2015**). "A lightweight yet sound-proof honeycomb acoustic metamaterial," Appl. Phys. Lett. **106**(17), 171905.
Urzhumov, Y., Ghezzo, F., Hunt, J., and Smith, D. R. (**2010**). "Acoustic cloaking transformations from attainable material properties," New J. Phys. **12**(7), 073014.
Venegas, G. R., and Wilson, P. S. (**2019**). "An illustration of the effect of neglecting poroelastic physics of water-saturated glass beads in a laboratory phase speed inference process," J. Acoust. Soc. Am. **146**(2), 1326–1334.
Wen-chao, H., and Chung-fai, N. (**1998**). "Sound insulation improvement using honeycomb sandwich panels," Appl. Acoust. **53**(1–3), 163–177.
Wood, A. (**1930**). *A Textbook of Sound* (George Bell & Sons, Edinburgh, UK).
Yazaki, T., Tashiro, Y., and Biwa, T. (**2007**). "Measurements of sound propagation in narrow tubes," Proc. R. Soc. A Math. Phys. Sci. **463**(2087), 2855–2862.
Yves, S., Fleury, R., Berthelot, T., Fink, M., Lemoult, F., and Lerosey, G. (**2017**). "Crystalline metamaterials for topological properties at subwavelength scales," Nat. Commun. **8**, 16023.
Zenkert, D. (**1995**). *An Introduction to Sandwich Construction* (Engineering Materials Advisory Services, London).
Zhang, S., Xia, C., and Fang, N. (**2011**). "Broadband acoustic cloak for ultrasound waves," Phys. Rev. Lett. **106**(2), 024301.
Zigoneanu, L., Popa, B.-I., and Cummer, S. A. (**2014**). "Three-dimensional broadband omnidirectional acoustic ground cloak," Nat. Mater. **13**(4), 352–355.